# USP20 Stabilizes FABP5 to Drive Macrophage Foam Cell Formation and Atherosclerosis

Man Zhang[1], Song Wang[1], Youyong Tang[1], Wei Qian[2], Xiaolin Yue[2], Yichi Zhang[1], Huiliang Cui[2], Yongxin Han[1], Siqiang Zhu[1], Tingting Liu[2], Yunshan Wang[1]*, Wencheng Zhang[2]* and Mo Wang[3]*

[1]Department of Clinical Laboratory, Shandong Provincial Hospital Affiliated to Shandong First Medical University, Jinan 250021, China.

[2]State Key Laboratory for Innovation and Transformation of Luobing Theory; Key Laboratory of Cardiovascular Remodeling and Function Research of MOE, NHC, CAMS and Shandong Province; Department of Cardiology, Qilu Hospital of Shandong University, Jinan 250012, China.

[3]Department of Vascular Surgery, Shandong Provincial Hospital Affiliated to Shandong First Medical University, Jinan 250021, China.

Man Zhang, Song Wang and Youyong Tang contributed equally to this work.

***Corresponding authors:**

Mo Wang, No. 324, Jingwu Weiqi Road, Huaiyin District, Jinan, Shandong, 250001, China. E-mail: wangmo@sph.com.cn.

Wencheng Zhang, No. 107, Wen Hua Xi Rd, Jinan, Shandong, 250012, China. Phone: 86-531-82169258. Fax: 86-531-82169257. E-mail: zhangwencheng@sdu.edu.cn; Yunshan Wang, No. 324, Jingwu Weiqi Road, Huaiyin District, Jinan, Shandong, 250001, China. Phone: 86-531-68779526. Fax: 86-531-68779526. E-mail: wangyunshansd@sdu.edu.cn.

**Abstract**

**Background:** Macrophage foam cell formation is a central event in atherosclerosis. Although protein ubiquitination is increasingly recognized as a regulator of macrophage lipid handling, whether deubiquitinating enzymes directly control lipid uptake and metabolic remodeling during atherogenesis remains unclear.

**Methods and Results:** Here, transcriptomic profiling identified ubiquitin-specific protease 20 (USP20) as a previously unrecognized regulator of macrophage foam cell formation. Genetic and pharmacological studies demonstrated that USP20 promoted macrophage lipid accumulation and foam cell formation, whereas macrophage-specific *Usp20* deficiency markedly attenuated atherosclerotic lesion formation, lipid deposition, and macrophage accumulation in mice. To elucidate the underlying mechanism, integrative analysis of USP20-interacting proteins and proteomic alterations in *Usp20*-deficient macrophages identified fatty acid-binding protein 5 (FABP5) as a substrate of USP20. Mechanistically, USP20 interacted with FABP5 and stabilized its protein abundance by preventing ubiquitin-dependent proteasomal degradation. Consequently, USP20-mediated stabilization of FABP5 enhanced PPARγ occupancy at the *Cd36* promoter, thereby increasing *Cd36* transcription, ox-LDL uptake, and foam cell formation. Accordingly, *Fabp5* knockdown abolished USP20-induced CD36 expression, ox-LDL uptake, and foam cell formation, whereas pharmacological activation of PPARγ restored CD36 expression in *Fabp5*-deficient macrophages. Finally, macrophage-targeted delivery of the USP20 inhibitor GSK2643943A markedly reduced atherosclerotic burden without evident systemic toxicity, supporting the therapeutic potential of targeting USP20 in atherosclerosis.

**Conclusions:** USP20 promotes macrophage foam cell formation by stabilizing FABP5 and enhancing PPARγ-dependent *Cd36* transcription. Targeting the USP20–FABP5-PPARγ–CD36 axis may represent a therapeutic strategy to limit macrophage lipid accumulation, metabolic dysfunction, and atherosclerosis progression.

**Keywords:** Atherosclerosis, macrophage, USP20, FABP5, CD36

**Novelty and Significance:**

52 **What Is Known?**

53 • Macrophage lipid accumulation and foam cell formation are critical events in the
54 development and progression of atherosclerosis.

55 • CD36-mediated uptake of ox-LDL contributes substantially to macrophage foam
56 cell formation, and its expression is regulated by PPARγ-dependent transcription.

57 • FABP5 participates in intracellular lipid handling and PPAR signaling, but its
58 function in macrophages is context dependent, and the mechanisms controlling FABP5
59 protein stability during atherosclerosis remain poorly understood.

60 **What New Information Does This Article Contribute?**

61 • Macrophage USP20 promotes foam cell formation and atherosclerosis, whereas
62 macrophage-specific *Usp20* deletion attenuates atherosclerotic lesion development.

63 • USP20 deubiquitinates and stabilizes FABP5, thereby enhancing PPARγ-
64 dependent *Cd36* transcription and promoting ox-LDL uptake and lipid accumulation in
65 macrophages.

66 • Pharmacological inhibition of USP20 using a macrophage-targeted nano-delivery
67 system suppresses foam cell formation and attenuates experimental atherosclerosis,
68 supporting USP20 as a potential therapeutic target.

69 **Introduction**

70 Atherosclerosis (AS) is a chronic inflammatory disease characterized by
71 progressive lipid deposition within the arterial wall and remains the leading cause of
72 cardiovascular morbidity and mortality worldwide[1, 2]. Macrophages are central
73 regulators throughout the initiation and progression of atherosclerotic lesions[3, 4].
74 Excessive uptake of modified lipoproteins, particularly oxidized low-density
75 lipoprotein (ox-LDL), drives macrophage foam cell formation, one of the earliest

pathological hallmarks of atherosclerotic lesion development[5-7]. Beyond serving as reservoirs for accumulated lipids, foam cells promote chronic inflammation, apoptosis, necrotic core formation, and plaque progression[8]. Consequently, elucidating the molecular mechanisms governing macrophage foam cell formation remains a major objective for developing effective therapeutic strategies against atherosclerotic cardiovascular disease.

Foam cell formation is determined by the balance between lipid uptake and cholesterol efflux[9]. Modified lipoproteins are internalized through multiple scavenger receptors, including CD36, scavenger receptor A1 (SR-A1/MSR1), and lectin-like oxidized low-density lipoprotein receptor-1 (LOX-1), whereas cholesterol efflux is primarily mediated by ATP-binding cassette transporters (ABCA1 and ABCG1) and scavenger receptor class B type I (SR-B1/SCARB1)[10, 11]. Disturbance of this coordinated network results in excessive intracellular cholesterol accumulation and foam cell formation[12]. Among these lipid-handling proteins, CD36 is recognized as the predominant receptor responsible for macrophage ox-LDL uptake and plays a pivotal role in atherosclerotic lesion development[13-15]. Intracellular lipid handling also depends on a variety of lipid-binding proteins that facilitate fatty acid trafficking and metabolic signaling[16, 17]. Among these, fatty acid-binding protein 5 (FABP5) has been implicated in lipid metabolism, inflammatory responses, and cardiovascular diseases[18]. Although the biological functions of these receptors and transporters have been extensively characterized, the upstream molecular mechanisms coordinating macrophage lipid handling remain incompletely understood.

Protein ubiquitination is a reversible post-translational modification that regulates protein stability, localization, and activity through the coordinated actions of E3 ubiquitin ligases and deubiquitinating enzymes (DUBs)[19, 20]. Increasing evidence suggests that ubiquitin signaling plays a pivotal role in macrophage lipid metabolism and atherosclerosis[21, 22]. Recent studies have demonstrated that E3 ubiquitin ligases regulate key lipid-handling proteins involved in cholesterol efflux and lipoprotein uptake, including ABCA1, LOX-1, and SR-B1, thereby influencing macrophage foam

cell formation and atherosclerosis[23-25]. These findings underscore ubiquitin-mediated regulation as a critical mechanism governing macrophage lipid homeostasis. However, compared with E3 ubiquitin ligases, the roles of deubiquitinating enzymes in macrophage foam cell formation remain largely unexplored. Ubiquitin-specific protease 20 (USP20), a member of the USP family of deubiquitinating enzymes, has been reported to participate in inflammatory signaling and metabolic regulation in several biological contexts[26-28]. Our previous study further demonstrated that USP20 promotes endoplasmic reticulum (ER)-phagy by deubiquitinating and stabilizing the ER-phagy receptor FAM134B/RETREG1[29]. However, whether USP20 regulates macrophage lipid metabolism and foam cell formation during atherosclerosis remains unknown.

In the present study, we performed transcriptomic profiling of macrophage foam cells to systematically identify deubiquitinating enzymes associated with lipid accumulation and identified USP20 as a previously unrecognized candidate regulator. Using macrophage-specific *Usp20* knockout mice, we demonstrated that *Usp20* deficiency attenuated macrophage foam cell formation and atherosclerotic lesion development. Through integrated quantitative proteomics, immunoprecipitation–mass spectrometry, and mechanistic studies, we further revealed that USP20 promotes foam cell formation by stabilizing fatty acid-binding protein 5 (FABP5), thereby enhancing PPARγ-dependent *Cd36* transcription. Furthermore, pharmacological inhibition of USP20 using GSK2643943A-loaded metal–organic framework (MOF) nanoparticles markedly attenuated experimental atherosclerosis, supporting USP20 as a potential therapeutic target for atherosclerotic cardiovascular disease.

## Methods

### Data Availability

The data supporting the findings of this study are available from the corresponding author upon reasonable request. RNA sequencing and proteomic datasets generated during this study will be deposited in the Gene Expression Omnibus (GEO) and ProteomeXchange repositories before publication.

134 **Animals**

135 Macrophage-specific *Usp20* knockout mice were generated by crossing *Usp20*$^{fl/fl}$
136 mice with *Lyz2*-Cre mice. Atherosclerosis was induced by a single tail-vein injection of
137 recombinant adeno-associated virus carrying the murine proprotein convertase
138 subtilisin/kexin type 9 mutant (AAV-*PCSK9*$^{D377Y}$; $2 \times 10^{11}$ genome copies (GC) per
139 mouse), followed by Paigen diet feeding for 12 weeks, as previously described[30]. For
140 therapeutic studies, mice received macrophage-targeted GSK2643943A-loaded MOF
141 nanoparticles or the corresponding control formulation by intravenous injection
142 according to the indicated schedule. At the experimental endpoint, blood, aortas, and
143 aortic roots were collected for biochemical and histological analyses, while major
144 organs were harvested for histopathological evaluation of systemic biosafety. All
145 animal experiments were approved by the Laboratory Animal Ethics Committee of Qilu
146 Hospital of Shandong University (approval No. DWLL-202400095) and were
147 conducted in accordance with institutional guidelines for the care and use of laboratory
148 animals.

149 **Human specimens**

150 Formalin-fixed human carotid atherosclerotic plaque specimens were obtained
151 from patients undergoing carotid endarterectomy at Shandong Provincial Hospital. For
152 each patient, paired atherosclerotic plaque regions and adjacent macroscopically non-
153 plaque arterial regions from the same carotid specimen were selected for histological
154 analysis. The non-plaque arterial regions were defined as plaque-adjacent areas without
155 macroscopically evident atherosclerotic lesions and served as paired internal controls.
156 Paraffin-embedded tissues were sectioned at a thickness of 5 μm and subjected to
157 immunofluorescence staining for USP20 and cell type-specific markers, including
158 CD68, α-SMA, and CD31. The use of human specimens was approved by the
159 Biomedical Research Ethics Committee of Shandong Provincial Hospital (approval No.
160 SWYX:NO.2026-896). The requirement for informed consent was waived by the ethics
161 committee.

162 **Cell Culture and Treatments**

Bone marrow-derived macrophages were isolated from mice and differentiated in macrophage colony-stimulating factor-containing medium. Foam cell formation was induced by treatment with oxidized low-density lipoprotein. Gene expression was modulated by siRNA-mediated knockdown or adenovirus-mediated overexpression. Where indicated, cells were treated with GSK2643943A, rosiglitazone, GW501516, cycloheximide, MG132, or chloroquine. Concentrations and treatment durations are provided in the figure legends and Supplemental Methods.

**Histological and lipid accumulation analyses**

Atherosclerotic lesion burden was assessed by en face Oil Red O staining of the aorta and Oil Red O staining of aortic root sections. Plaque morphology and macrophage content were evaluated by hematoxylin and eosin staining and immunofluorescence staining, respectively. Images were quantified using ImageJ by investigators blinded to group allocation.

**RNA and protein analyses**

Total RNA was isolated and analyzed by quantitative reverse-transcription PCR using gene-specific primers. Relative gene expression was calculated using the $2^{-\Delta\Delta Ct}$ method. Protein abundance was assessed by immunoblotting using the indicated antibodies, and band intensities were quantified by densitometry. Primer and antibody information is provided in the Supplemental Tables.

**Foam cell formation, lipid uptake, and cholesterol efflux assays**

Macrophage lipid accumulation was evaluated by Oil Red O staining, and ox-LDL uptake was assessed using DiI-labeled ox-LDL. Fluorescence intensity and lipid-positive area were quantified using ImageJ and normalized to cell number. Cholesterol efflux was assessed by loading macrophages with NBD-cholesterol, followed by incubation with HDL as the cholesterol acceptor. Cholesterol efflux was calculated as the percentage of fluorescence in the medium relative to the total fluorescence in the medium and cells.

**RNA sequencing and quantitative proteomic analysis**

Total RNA and proteins were extracted from macrophages using standard

192 procedures. RNA sequencing libraries were generated and sequenced on an Illumina
193 platform. Differentially expressed genes were identified using DESeq2, followed by
194 Gene Ontology (GO) and Kyoto Encyclopedia of Genes and Genomes (KEGG)
195 enrichment analyses.

196 For quantitative proteomic analysis, tryptic peptides were labeled with tandem
197 mass tags (TMT) and analyzed by liquid chromatography–tandem mass spectrometry
198 (LC-MS/MS). Differentially expressed proteins were subjected to GO, KEGG, and
199 Gene Set Enrichment Analysis (GSEA) to identify biological pathways altered by
200 *Usp20* deficiency.

201 **Immunoblotting and co-immunoprecipitation**

202 Total cellular proteins were extracted using lysis buffer containing protease
203 inhibitors. Equal amounts of protein were subjected to SDS-PAGE followed by
204 immunoblotting using the indicated primary antibodies. Protein bands were visualized
205 by enhanced chemiluminescence and quantified by densitometric analysis. Protein-
206 protein interactions were examined by co-immunoprecipitation. Cell lysates were
207 incubated with the indicated antibodies followed by Protein A/G agarose beads.
208 Immunoprecipitated proteins were detected by immunoblotting.

209 **Ubiquitination and protein stability assays**

210 Ubiquitination assays were performed as previously described[29]. Briefly, cells
211 were transfected with HA-tagged ubiquitin together with the indicated expression
212 constructs. Where indicated, cells were treated with the proteasome inhibitor MG132
213 before harvesting. Cell lysates were prepared under denaturing conditions, and
214 ubiquitinated FABP5 was detected by immunoprecipitation followed by
215 immunoblotting.

216 Protein stability was evaluated using cycloheximide (CHX) chase assays. Cells
217 were harvested at the indicated time points after inhibition of protein synthesis, and
218 FABP5 protein degradation was analyzed by immunoblotting.

219 **Chromatin immunoprecipitation**

220 Chromatin immunoprecipitation (ChIP) assays were performed to evaluate PPARγ

binding to the *Cd36* promoter. Briefly, cells were cross-linked with formaldehyde, lysed, and sonicated to generate chromatin fragments of approximately 200–500 bp. Chromatin was immunoprecipitated using an anti-PPARγ antibody or control IgG. Purified DNA was analyzed by quantitative PCR using primers spanning the predicted PPARγ-binding region within the *Cd36* promoter. ChIP enrichment was quantified by qPCR and normalized to the corresponding input DNA. Specific enrichment at the CD36 promoter was calculated by dividing the %Input value of the target region by that of a negative control region lacking predicted PPARγ-binding sites.

**Seahorse metabolic analysis**

Extracellular acidification rate (ECAR) and oxygen consumption rate (OCR) were measured using an extracellular flux analyzer according to the manufacturer's instructions. Glycolytic and mitochondrial stress tests were performed to evaluate glycolytic function and mitochondrial respiration. Metabolic parameters were calculated using Wave software. Mitochondrial reactive oxygen species were detected using MitoSOX staining according to the manufacturer's instructions.

**Preparation of macrophage-targeted GSK2643943A-loaded MOF nanoparticles**

GSK2643943A-loaded MOF nanoparticles were prepared using a previously established method with minor modifications and functionalized for macrophage-targeted delivery[31]. Particle size, morphology, and drug loading were evaluated as described in the Supplemental Methods.

**Statistical analysis**

Data are presented as mean ± SEM unless otherwise indicated. Statistical analyses were performed using GraphPad Prism. Comparisons between two groups were analyzed using paired or unpaired two-tailed Student's t tests, as appropriate. Comparisons among multiple groups were performed using one-way or two-way ANOVA followed by appropriate post hoc multiple-comparison tests. Values of $P < 0.05$ were considered statistically significant.

Animals and samples were randomly assigned to experimental groups whenever applicable. Investigators performing quantitative image analyses were blinded to

genotype and treatment. No statistical method was used to predetermine sample size, and no samples or animals were excluded unless predefined exclusion criteria were met.

## Results

### USP20 is upregulated during macrophage foam cell formation and atherosclerosis

To identify deubiquitinating enzymes potentially involved in macrophage foam cell formation, we first performed RNA sequencing in bone marrow-derived macrophages (BMDMs) treated with ox-LDL. Transcriptomic analysis revealed extensive gene expression changes induced by lipid loading (**Figure 1A** and **Figure S1A–B**). Among the differentially expressed DUBs, several ubiquitin-specific proteases were altered in response to ox-LDL treatment, with USP20 showing one of the most pronounced increases (**Figure 1B**). Consistently, ox-LDL stimulation induced a time-dependent increase in USP20 protein and mRNA expression in macrophages (**Figure 1C–E**). Immunofluorescence staining further confirmed increased USP20 expression in foam cells induced by ox-LDL (**Figure S1C**). Although USP20 has previously been implicated in vascular smooth muscle cell function during atherosclerosis, its role in macrophage lipid metabolism remains unknown[32, 33]. We therefore investigated the function of macrophage USP20 in foam cell formation and atherosclerosis.

To investigate the relationship between USP20 expression and atherosclerotic lesion progression *in vivo*, we examined USP20 expression in AAV-*PCSK9*$^{D377Y}$-induced atherosclerotic mice during disease progression. Immunofluorescence staining revealed that USP20 expression increased progressively throughout Paigen diet feeding and was predominantly localized to MOMA-2$^{+}$ macrophages within atherosclerotic lesions (**Figure 1F–H**). To validate these findings in human disease, we next examined formalin-fixed paraffin-embedded carotid endarterectomy specimens. Compared with paired adjacent non-plaque arterial regions from the same patients, carotid atherosclerotic plaques exhibited markedly elevated USP20 expression, which showed extensive colocalization with CD68$^{+}$ macrophages (**Figure 1I–K**). In contrast, USP20 displayed only limited colocalization with α-SMA$^{+}$ vascular smooth muscle cells or

279 CD31$^{+}$ endothelial cells (**Figure S1E–F**), suggesting that increased USP20 expression
280 within human atherosclerotic plaques is predominantly associated with macrophage-
281 rich regions.

282 Collectively, these findings demonstrate that USP20 is progressively upregulated
283 during macrophage foam cell formation and atherosclerotic plaque development,
284 identifying USP20 as a candidate regulator of macrophage-driven atherogenesis.

285 **Macrophage-specific deletion of *Usp20* attenuates atherosclerosis**

286 Given the marked upregulation of USP20 in plaque macrophages, we next
287 investigated its functional role in atherosclerosis by generating macrophage-specific
288 *Usp20* knockout (*Usp20*$^{MacKO}$) mice through crossing *Usp20*$^{fl/fl}$ mice with *Lyz2*-Cre
289 mice (**Figure 2A**). Efficient deletion of *Usp20* in BMDMs isolated from *Usp20*$^{MacKO}$
290 mice was confirmed by both Western blotting and RT-qPCR (**Figure 2B–D**). To
291 determine the role of macrophage USP20 in atherosclerotic lesion development,
292 *Usp20*$^{MacKO}$ mice and littermate *Usp20*$^{fl/fl}$ controls were subjected to AAV-*PCSK9*$^{D377Y}$
293 induced atherosclerosis followed by Paigen diet feeding. En face Oil Red O staining
294 revealed a marked reduction in atherosclerotic lesion area throughout the aorta of
295 *Usp20*$^{MacKO}$ mice compared with control mice (**Figure 2E–F**). Consistently,
296 histological analysis of aortic root sections demonstrated significantly smaller plaques,
297 reduced lipid deposition, and diminished macrophage accumulation, as evidenced by a
298 reduced MOMA-2$^{+}$ area **(Figure 2G–J**).

299 Similar protective effects were observed in female mice, in which macrophage-
300 specific *Usp20* deficiency significantly reduced aortic lesion burden, aortic root plaque
301 area, lipid accumulation, and macrophage infiltration compared with *Usp20*$^{fl/fl}$ controls
302 (**Figure S2A–F**). Importantly, macrophage-specific *Usp20* deficiency did not
303 significantly alter body weight or circulating lipid profiles in either male or female mice
304 (**Figure 2K–O** and **Figure S2G**), indicating that the reduction in atherosclerosis was
305 unlikely to result from systemic alterations in lipid metabolism.

306 Collectively, these findings demonstrate that macrophage USP20 promotes
307 atherosclerotic plaque development and macrophage accumulation within lesions,

independent of systemic changes in lipid metabolism.

**USP20 promotes macrophage foam cell formation by enhancing CD36-mediated ox-LDL uptake**

Having established a pro-atherogenic role for macrophage USP20 *in vivo*, we next investigated whether USP20 regulates macrophage foam cell formation. Adenoviral overexpression of *Usp20* markedly increased ox-LDL-induced lipid accumulation in BMDMs, as evidenced by enhanced Oil Red O staining (**Figure 3A–B**). Conversely, macrophages from *Usp20*$^{MacKO}$ mice exhibited significantly reduced intracellular lipid accumulation following ox-LDL stimulation (**Figure 3C–D**), indicating that USP20 promotes macrophage foam cell formation.

We next determined whether USP20 affects lipid uptake or cholesterol efflux. DiI-labeled ox-LDL uptake assays revealed markedly reduced ox-LDL internalization in *Usp20*-deficient macrophages compared with control cells (**Figure 3E–F**). In contrast, HDL-mediated cholesterol efflux was comparable between *Usp20*$^{fl/fl}$ and *Usp20*$^{MacKO}$ macrophages (**Figure 3G–H**), suggesting that USP20 primarily regulates lipid uptake rather than cholesterol efflux. To identify the molecular basis of this effect, we examined major scavenger receptors and cholesterol transporters involved in macrophage lipid homeostasis. Among the proteins analyzed, CD36 expression was markedly decreased in *Usp20*-deficient macrophages, whereas SR-A1, LOX-1, ABCA1, ABCG1, and SR-B1 remained largely unchanged (**Figure 3I–J**). These findings indicate that USP20 promotes macrophage foam cell formation by selectively enhancing CD36-dependent ox-LDL uptake.

***Usp20* deficiency reshapes macrophage metabolic programs**

To investigate the downstream consequences regulated by USP20 in macrophages, we performed quantitative proteomic analysis of control and *Usp20*-deficient macrophages. Pathway enrichment analysis revealed that metabolic pathways were prominently altered by *Usp20* deletion (**Figure 4A** and **Figure S3A–D**). KEGG and GSEA analyses further revealed suppression of glycolysis/gluconeogenesis and enhancement of oxidative phosphorylation-related pathways in *Usp20*-deficient

macrophages (**Figure 4A–B**). Consistent with these findings, heatmap analysis demonstrated coordinated downregulation of glycolytic proteins and upregulation of proteins involved in oxidative phosphorylation (**Figure 4C**).

To determine whether these proteomic changes were accompanied by functional metabolic reprogramming, we performed Seahorse extracellular flux analysis. *Usp20* silencing markedly reduced extracellular acidification rate (ECAR), including basal glycolysis, glycolytic capacity, and glycolytic reserve (**Figure 4D–E**). In contrast, oxygen consumption rate (OCR) was significantly increased accompanied by elevated basal respiration, maximal respiration, and OCR/ECAR ratio (**Figure 4F–H**). These findings indicate that loss of *Usp20* reprograms macrophage metabolism from glycolysis toward oxidative phosphorylation, consistent with previous reports demonstrating that acute ox-LDL stimulation induces a metabolic shift from oxidative phosphorylation toward glycolysis in macrophages[34, 35]. We next examined mitochondrial oxidative stress using MitoSOX staining. Ox-LDL stimulation markedly increased mitochondrial ROS production in control macrophages, whereas this response was significantly attenuated in *Usp20*-deficient macrophages (**Figure 4I–J**). Collectively, these findings demonstrate that *Usp20* deficiency reprograms macrophage metabolism toward oxidative phosphorylation while alleviating mitochondrial oxidative stress during foam cell formation.

**USP20 stabilizes FABP5 through deubiquitination**

To identify the molecular substrate through which USP20 regulates macrophage foam cell formation, we integrated USP20 immunoprecipitation-mass spectrometry (IP-MS) with quantitative proteomic analysis of *Usp20*-deficient macrophages. Cross-analysis of these datasets identified five candidate proteins that both interacted with USP20 and were downregulated following *Usp20* deletion (**Figure 5A**). Among these candidates, we focused on FABP5 because previous studies have implicated FABP5 in atherosclerotic cardiovascular disease and demonstrated its role in regulating the balance between glycolysis and oxidative phosphorylation in immune cells[36, 37]. These observations suggested that FABP5 could represent a molecular link between USP20

366 and macrophage metabolic reprogramming.

367 Reciprocal co-immunoprecipitation assays confirmed an interaction between
368 USP20 and FABP5 in HEK293T cells (**Figure 5B–C**), which was further validated by
369 endogenous co-immunoprecipitation in macrophages (**Figure 5D**). Molecular docking
370 analysis supported a stable interaction between USP20 and FABP5 (**Figure S4A**), and
371 confocal microscopy revealed extensive intracellular colocalization of the two proteins
372 (**Figure S4B–C**). Because USP20 is a deubiquitinating enzyme, we next examined
373 whether it regulates FABP5 ubiquitination. Wild-type USP20 markedly reduced FABP5
374 ubiquitination, whereas this effect was abolished by the catalytically inactive
375 *C153S/H643Q* mutation (**Figure 5E** and **Figure S5A**), demonstrating that USP20-
376 mediated deubiquitination of FABP5 is dependent on its catalytic activity.
377 Ubiquitination assays using linkage-specific ubiquitin mutants further demonstrated
378 that USP20 selectively reduced K48-linked, but not K63-linked, polyubiquitination of
379 FABP5 (**Figure 5F**), indicating that USP20 preferentially removes degradation-
380 associated K48-linked ubiquitin chains from FABP5. We next determined whether
381 USP20-mediated deubiquitination affects FABP5 protein stability. Macrophage-
382 specific deletion of *Usp20* markedly reduced endogenous FABP5 protein abundance
383 without affecting its mRNA levels (**Figure 5G–H** and **Figure S5B**). Consistently,
384 cycloheximide chase assays showed that *Usp20* overexpression significantly prolonged
385 the half-life of FABP5 (**Figure 5I–J**). Furthermore, treatment with the proteasome
386 inhibitor MG132 restored FABP5 protein levels in *Usp20*-deficient macrophages,
387 whereas the lysosomal inhibitor chloroquine had little effect (**Figure 5K** and **Figure**
388 **S5C**). Together, these findings demonstrate that USP20 stabilizes FABP5 by removing
389 K48-linked polyubiquitin chains and preventing proteasome-dependent degradation.
390 Immunofluorescence staining and nuclear–cytoplasmic fractionation further showed
391 that *Usp20* deficiency did not substantially alter the intracellular distribution of FABP5
392 (**Figure S5D–E**), indicating that USP20 primarily regulates FABP5 protein stability
393 rather than its subcellular localization. To identify the FABP5 ubiquitination site
394 targeted by USP20, we selected four lysine residues (K24, K34, K40, and K61) based

395 on their evolutionary conservation and previously reported ubiquitination sites curated
396 in the PhosphoSitePlus database. Lysine-to-arginine mutants were subsequently
397 generated and subjected to ubiquitination assays. Notably, the *K34R* mutation largely
398 abolished USP20-mediated deubiquitination of FABP5, whereas mutations at K24, K40,
399 or K61 had minimal effects (**Figure 5L**). These findings identify Lys34 as a key residue
400 required for USP20-mediated regulation of FABP5 ubiquitination.

401 **FABP5 mediates USP20-dependent activation of the PPARγ–CD36 axis and**
402 **macrophage foam cell formation.**

403 Having established FABP5 as a direct substrate of USP20, we next investigated
404 how FABP5 promotes macrophage foam cell formation. Consistent with previous
405 studies showing that FABP5 is highly enriched in lipid-associated macrophages within
406 atherosclerotic plaques[38, 39], immunofluorescence staining demonstrated that FABP5
407 was highly expressed in MOMA-2$^{+}$ macrophages (**Figure 6A**). Consistent with this
408 observation, silencing *Fabp5* markedly reduced ox-LDL-induced lipid accumulation in
409 macrophages, as demonstrated by Oil Red O staining (**Figure 6B–C**).

410 To identify the downstream targets regulated by FABP5, we examined the
411 expression of scavenger receptors and cholesterol transporters involved in macrophage
412 lipid metabolism. Among these molecules, CD36 was significantly reduced following
413 *Fabp5* knockdown at both the protein and mRNA levels, whereas the expression of
414 LOX-1, SR-A1, ABCA1, ABCG1, and SR-B1 remained largely unchanged (**Figure**
415 **6D–F**), suggesting that FABP5 selectively regulates CD36 expression. FABP5
416 functions as an intracellular lipid chaperone and has been implicated in the regulation
417 of PPAR signaling in a cell type–dependent manner[17, 40]. Given the established role of
418 PPARγ in *CD36* transcription and the reported involvement of PPARβ/δ in macrophage
419 lipid metabolism[41, 42], we examined which PPAR pathway mediated FABP5-dependent
420 regulation of CD36. Activation of PPARγ with rosiglitazone (Rg), but not activation of
421 PPARβ/δ with GW501516 (GW), restored CD36 protein expression in *Fabp5* silenced
422 macrophages (**Figure 6G–H**). Consistent with these findings, ChIP-qPCR
423 demonstrated that *Fabp5* knockdown markedly reduced PPARγ enrichment at the *Cd36*

promoter (**Figure 6I–J**), indicating that FABP5 promotes *Cd36* transcription by facilitating PPARγ binding to its promoter.

To determine whether FABP5 mediates the pro-atherogenic function of USP20, rescue experiments were performed by overexpressing *Usp20* in control or *Fabp5*-deficient macrophages. *Usp20* overexpression markedly increased CD36 protein expression (**Figure 6K–L**), as well as ox-LDL uptake and foam cell formation (**Figure 6M–N**); however, these effects were largely abolished following *Fabp5* silencing. These findings establish FABP5 as the essential downstream effector of USP20 in promoting macrophage foam cell formation. Collectively, these results demonstrate that USP20 stabilizes FABP5, thereby enhancing PPARγ-dependent transcriptional activation of *Cd36* and promoting macrophage lipid uptake and foam cell formation.

**Macrophage-targeted delivery of the USP20 inhibitor GSK2643943A attenuates foam cell formation and atherosclerosis**

Having established the critical role of the USP20–FABP5-PPARγ–CD36 axis in macrophage foam cell formation, we next investigated whether pharmacological inhibition of USP20 could confer therapeutic benefit. Dose-response and cell viability analyses identified 5 μM GSK2643943A as an effective concentration that suppressed ox-LDL-induced lipid accumulation without compromising macrophage viability (**Figure 7A–B** and **Figure S6A–C**). Consistent with the phenotype observed in *Usp20*-deficient macrophages, GSK2643943A markedly attenuated foam cell formation and selectively reduced CD36 protein expression, without significantly affecting other lipid uptake or cholesterol efflux receptors, including SR-A1, LOX-1, ABCA1, ABCG1, and SR-B1 (**Figure S6D–E**). GSK2643943A treatment also significantly decreased FABP5 protein abundance (**Figure 7C–D**), further supporting the conclusion that pharmacological inhibition of USP20 destabilizes FABP5.

To evaluate the therapeutic efficacy of USP20 inhibition *in vivo*, we developed macrophage-targeted GSK2643943A-loaded MOF nanoparticles (GSK-MOF@DS) based on a previously established delivery platform[31]. TEM images showed that both MOF and GSK-MOF@DS retained an elongated, rod-like morphology after GSK

453 loading and subsequent DS modification (**Figure S7A**). The PXRD pattern of the
454 pristine MOF exhibited characteristic low-angle reflections at approximately 2θ = 2.4°,
455 4.8°, 7.1°, and 9.6°, consistent with the well-ordered crystalline framework of the parent
456 material (**Figure S7B**). DLS analysis of the MOF dispersed in water gave a
457 predominant hydrodynamic size population with a volume-weighted D50 of 154.2 ±
458 10.5 nm (**Figure S7C**). The zeta potential shifted from +23.86 ± 0.20 mV to +4.02 ±
459 0.27 mV upon GSK loading and reversed to −43.14 ± 0.80 mV after DS modification
460 (**Figure S7D**), reflecting the introduction of negatively charged sulfate groups onto the
461 particle surface. In the FTIR spectra, GSK-MOF@DS retained the MOF-associated
462 bands at approximately 1604 and 1405 $cm^{-1}$ and displayed additional bands at
463 approximately 1261, 1018, and 802 $cm^{-1}$ (**Figure S7E**), assigned to the sulfate and
464 glycosidic vibrations of DS. These spectral features, together with the charge reversal,
465 confirm the DS-mediated surface modification of GSK-MOF. GSK in anhydrous
466 ethanol exhibited a broad absorption band centered at approximately 356 nm, and the
467 absorbance increased with GSK concentration (**Figure S7F**). The absorbance at 390
468 nm, rather than at the absorption maximum, was used for quantification because it
469 afforded a more stable linear response, increasing linearly with GSK concentration over
470 0.047–3.0 mg/mL (**Figure S7G**). The drug-loading content of GSK-MOF, calculated
471 from the difference between the GSK feed and the unbound GSK recovered in the
472 pooled supernatant and washing fractions, was 16.78%. Together, the preserved
473 morphology, charge reversal, characteristic FTIR signatures, and drug-loading content
474 demonstrate the successful fabrication of GSK-MOF@DS.

475 To investigate the therapeutic potential of GSK-MOF@DS in atherosclerosis,
476 nanoparticles were intravenously administered twice weekly to AAV-*PCSK9*$^{D377Y}$–
477 induced atherosclerotic mice during Paigen diet feeding (**Figure 7E**). Compared with
478 saline-treated mice and mice receiving empty MOF@DS nanoparticles, GSK-
479 MOF@DS treatment markedly reduced atherosclerotic plaque burden, as demonstrated
480 by en face Oil Red O staining of the whole aorta (**Figure 7F–G**). Histological analyses
481 of aortic root sections further revealed significant reductions in lesion area, lipid

482 deposition, and macrophage accumulation, as assessed by H&E, Oil Red O, and
483 MOMA-2 staining, respectively (**Figure 7H–K**). These findings indicate that
484 macrophage-targeted pharmacological inhibition of USP20 effectively limits
485 atherosclerotic lesion progression. The in vivo biocompatibility of GSK-MOF@DS
486 was subsequently assessed by monitoring body weight, serum lipid profiles, hepatic
487 and renal function, and histological changes in major organs. No significant differences
488 were observed among the treatment groups in body weight or plasma TC, TG, HDL-C,
489 and LDL-C levels (**Figure S8A–B**). Serum ALT, AST, BUN, and creatinine levels also
490 remained comparable among groups (**Figure S8D – G)**. Moreover, histological
491 examination of the liver, spleen, lung, and kidney revealed no overt pathological
492 abnormalities following GSK-MOF@DS administration (**Figure S8C**). Together, these
493 results indicate that macrophage-targeted delivery of GSK2643943A attenuates
494 atherosclerosis without causing detectable systemic toxicity under the conditions
495 examined.

496 Collectively, these findings demonstrate that pharmacological targeting of the
497 USP20–FABP5 axis suppresses macrophage foam cell formation and atherosclerotic
498 lesion development, supporting USP20 as a potential therapeutic target for
499 atherosclerosis.

500 **Discussion**

501 The present study identifies USP20 as a previously unrecognized driver of
502 macrophage foam cell formation and atherosclerosis. USP20 was upregulated during
503 foam cell formation and in atherosclerotic lesions, where it directly deubiquitinated and
504 stabilized FABP5. This enhanced PPARγ occupancy at the *Cd36* promoter, increased
505 *Cd36* transcription, and promoted ox-LDL uptake and lesion development. Notably,
506 macrophage-targeted delivery of the USP20 inhibitor GSK2643943A reduced lipid
507 accumulation and attenuated experimental atherosclerosis, supporting USP20 as a
508 potential therapeutic target.

509 Although USP20 has been implicated in cardiovascular and metabolic regulation,

its role in macrophage lipid handling remains unclear. Previous studies have shown that USP20 suppresses inflammatory signaling in vascular smooth muscle cells through RIPK1 deubiquitination, promotes hepatic cholesterol synthesis by stabilizing HMGCR, and protects against pathological cardiac remodeling by removing K63-linked ubiquitin chains from STAT3 in cardiomyocytes[28, 32, 43]. These findings highlight the highly context- and substrate-dependent functions of USP20 across different cardiovascular and metabolic cell types. In contrast, our findings identify FABP5 as a previously unrecognized substrate of USP20 in macrophages, through which USP20 enhances PPARγ-dependent *Cd36* transcription and promotes foam cell formation. Unlike previously characterized substrates that primarily regulate inflammatory signaling, cholesterol biosynthesis, or cardiac remodeling, USP20-mediated stabilization of FABP5 directly promotes macrophage lipid uptake through the PPARγ–CD36 axis, thereby driving foam cell formation and atherosclerotic progression. These findings reveal a previously unrecognized macrophage-specific mechanism of USP20 action and broaden our understanding of how USP20 contributes to cardiovascular disease.

Accumulating evidence supports FABP5 as an intracellular lipid chaperone involved in fatty acid trafficking, lipid metabolism, and nuclear receptor signaling[18]. Clinical studies have linked elevated circulating FABP5 levels to adverse cardiometabolic profiles and greater atherosclerotic burden, as reflected by carotid intima-media thickness and coronary artery calcification[44-46]. However, whether FABP5 directly contributes to atherogenesis or merely serves as a circulating marker remains unclear. Moreover, previous experimental studies have yielded inconsistent findings regarding its function in macrophage biology[36, 47-49], leaving its precise role in macrophage foam cell formation incompletely understood. Prior studies identified TRIM45-mediated ubiquitination and USP14-dependent deubiquitination as context-specific regulators of FABP5[50, 51], but whether a distinct deubiquitinase controls FABP5 stability in macrophages was unknown. By integrating quantitative proteomics with immunoprecipitation–mass spectrometry, we identified FABP5 as a direct substrate of USP20. USP20 removed K48-linked ubiquitin chains from FABP5, prevented its

539 proteasomal degradation, and prolonged its protein stability (**Figure 5**). Functionally,
540 *Fabp5* depletion reduced PPARγ occupancy at the *Cd36* promoter and decreased CD36
541 expression (**Figure 6I–J**). Moreover, *Usp20* overexpression failed to restore CD36 after
542 *Fabp5* silencing (**Figure 6K–N**), establishing FABP5 as an essential downstream
543 mediator. Together, these findings define a previously unrecognized USP20–FABP5-
544 PPARγ–CD36 axis that promotes macrophage ox-LDL uptake and foam cell formation.
545 The selective effect of the USP20–FABP5 axis on CD36 expression provides
546 further insight into its role in macrophage lipid handling. USP20 inhibition reduced
547 CD36 expression without significantly affecting other lipid uptake or cholesterol efflux
548 receptors, including SR-A1, LOX-1, ABCA1, ABCG1, and SR-B1 (**Figure 3I–J**). This
549 selectivity likely reflects differences in the transcriptional control of these genes.
550 Although several scavenger receptors and cholesterol transporters can be influenced by
551 PPAR signaling under specific conditions, CD36 is a well-established direct
552 transcriptional target of PPARγ, whereas ABCA1 and ABCG1 are regulated
553 predominantly by LXR-dependent transcriptional programs, and SR-A1 and LOX-1 are
554 primarily controlled by inflammatory signaling pathways[41, 52-54]. Consistent with these
555 regulatory differences, *Fabp5* deficiency selectively reduced CD36 expression without
556 significantly affecting other lipid uptake or cholesterol efflux receptors. Accordingly,
557 the partial reduction in PPARγ activity caused by *Fabp5* depletion may preferentially
558 impair *Cd36* transcription while leaving other lipid-handling genes largely unaffected.
559 Consistent with this interpretation, ChIP-qPCR showed reduced PPARγ occupancy at
560 the *Cd36* promoter, suggesting that USP20-stabilized FABP5 promotes *Cd36*
561 transcription by facilitating PPARγ recruitment to its promoter. Whether the USP20–
562 FABP5 axis specifically promotes PPARγ recruitment to the *Cd36* promoter or more
563 generally influences promoter selection across distinct PPARγ target genes remains to
564 be determined.
565 Another important finding is that increased macrophage lipid accumulation was
566 accompanied by metabolic remodeling. Proteomic profiling identified glycolysis and
567 oxidative phosphorylation among the pathways most affected by *Usp20* deficiency, and

568 functional assays demonstrated reduced glycolytic activity together with preserved
569 mitochondrial respiration and lower mitochondrial oxidative stress (**Figure 4**). These
570 changes are unlikely to reflect a direct metabolic function of USP20. Previous studies
571 have shown that excessive ox-LDL uptake through CD36 promotes intracellular lipid
572 overload, impairs mitochondrial function, increases mitochondrial reactive oxygen
573 species, and shifts macrophage metabolism toward glycolysis[3, 34, 35]. Therefore,
574 suppression of the USP20–FABP5-PPARγ–CD36 axis would be expected to alleviate
575 lipid-induced metabolic stress, thereby preserving mitochondrial oxidative
576 phosphorylation and reducing glycolytic dependence.

577 Although intensive lipid lowering remains the cornerstone of contemporary
578 atherosclerosis management, substantial residual cardiovascular risk persists despite
579 current therapies, underscoring the need for complementary strategies that directly
580 target pathogenic processes within atherosclerotic plaques[55, 56]. Because macrophage
581 foam cell formation is driven by excessive modified-lipoprotein uptake and impaired
582 cholesterol handling, approaches targeting macrophage lipid accumulation have
583 emerged as promising therapeutic directions[57, 58]. Our findings identify USP20 as an
584 upstream regulator of this process by stabilizing FABP5 and enhancing PPARγ-
585 dependent *Cd36* transcription, thereby promoting ox-LDL uptake and foam cell
586 formation. Importantly, macrophage-targeted delivery of the USP20 inhibitor
587 GSK2643943A attenuated lipid accumulation, and atherosclerotic lesion development,
588 supporting macrophage-directed USP20 inhibition as a potential complementary
589 therapeutic strategy, particularly given the context-dependent functions of USP20 in
590 other tissues.

591 In conclusion, the present study identifies USP20 as a critical regulator of
592 macrophage lipid uptake and foam cell formation through stabilization of FABP5. By
593 enhancing PPARγ-dependent *Cd36* transcription, USP20 promotes ox-LDL uptake,
594 lipid accumulation, and atherosclerotic lesion development. Inhibition of USP20
595 effectively suppresses this signaling cascade and attenuates atherosclerosis. These
596 findings uncover a previously unrecognized USP20–FABP5-PPARγ–CD36 signaling

axis and provide a potential therapeutic strategy for the treatment of atherosclerotic cardiovascular disease.

**Acknowledgments**

None.

**Sources of Funding**

This study was supported by grants from the National Natural Science Foundation of China (Nos. 82600884 and 32402860), the Taishan Scholar Program of Shandong Province (Nos. tsqn202507353 and tstp20240852), the Natural Science Foundation of Shandong Province (Nos. ZR2024ZD18, ZR2024ZD23, and ZR2025MS1294), the Key Research and Development Program of Shandong Province (Major Scientific and Technological Innovation Project) (No. 2026CXGC010602), and the Open Fund of the National Innovation Center for Advanced Medical Devices (No. NMED2025KF-06-060).

**Disclosures**

None.

**References**

1. Libby P. The changing landscape of atherosclerosis. *Nature*. 2021;592:524-533.
2. Global Burden of Cardiovascular D and Risks C. Global, Regional, and National Burden of Cardiovascular Diseases and Risk Factors in 204 Countries and Territories, 1990-2023. *J Am Coll Cardiol*. 2025;86:2167-2243.
3. Moore KJ and Tabas I. Macrophages in the pathogenesis of atherosclerosis. *Cell*. 2011;145:341-55.
4. Moore KJ, Sheedy FJ and Fisher EA. Macrophages in atherosclerosis: a dynamic balance. *Nat Rev Immunol*. 2013;13:709-21.
5. Duan Y, Gong K, Xu S, Zhang F, Meng X and Han J. Regulation of cholesterol homeostasis in health and diseases: from mechanisms to targeted therapeutics. *Signal Transduct Target Ther*. 2022;7:265.
6. Ai J, Tang X, Zhou Y, Mao B, Zhang Q, Zhao J, Chen W and Cui S. New insights into foam cells in atherosclerosis. *Cardiovasc Res*. 2025;121:2334-2346.
7. Bhargava S, de la Puente-Secades S, Schurgers L and Jankowski J. Lipids and lipoproteins in cardiovascular diseases: a classification. *Trends Endocrinol Metab*. 2022;33:409-423.
8. Ajoolabady A, Pratico D, Lin L, Mantzoros CS, Bahijri S, Tuomilehto J and Ren J. Inflammation in atherosclerosis: pathophysiology and mechanisms. *Cell Death Dis*. 2024;15:817.

9. Yu XH, Fu YC, Zhang DW, Yin K and Tang CK. Foam cells in atherosclerosis. *Clin Chim Acta*. 2013;424:245-52.

10. Kzhyshkowska J, Neyen C and Gordon S. Role of macrophage scavenger receptors in atherosclerosis. *Immunobiology*. 2012;217:492-502.

11. Westerterp M, Bochem AE, Yvan-Charvet L, Murphy AJ, Wang N and Tall AR. ATP-binding cassette transporters, atherosclerosis, and inflammation. *Circ Res*. 2014;114:157-70.

12. Tall AR and Yvan-Charvet L. Cholesterol, inflammation and innate immunity. *Nat Rev Immunol*. 2015;15:104-16.

13. Febbraio M, Podrez EA, Smith JD, Hajjar DP, Hazen SL, Hoff HF, Sharma K and Silverstein RL. Targeted disruption of the class B scavenger receptor CD36 protects against atherosclerotic lesion development in mice. *J Clin Invest*. 2000;105:1049-56.

14. Silverstein RL and Febbraio M. CD36, a scavenger receptor involved in immunity, metabolism, angiogenesis, and behavior. *Sci Signal*. 2009;2:re3.

15. Shu H, Peng Y, Hang W, Nie J, Zhou N and Wang DW. The role of CD36 in cardiovascular disease. *Cardiovasc Res*. 2022;118:115-129.

16. Furuhashi M and Hotamisligil GS. Fatty acid-binding proteins: role in metabolic diseases and potential as drug targets. *Nat Rev Drug Discov*. 2008;7:489-503.

17. Storch J and Corsico B. The emerging functions and mechanisms of mammalian fatty acid-binding proteins. *Annu Rev Nutr*. 2008;28:73-95.

18. Xu B, Chen L, Zhan Y, Marquez KNS, Zhuo L, Qi S, Zhu J, He Y, Chen X, Zhang H, Shen Y, Chen G, Gu J, Guo Y, Liu S and Xie T. The Biological Functions and Regulatory Mechanisms of Fatty Acid Binding Protein 5 in Various Diseases. *Front Cell Dev Biol*. 2022;10:857919.

19. Clague MJ, Urbe S and Komander D. Breaking the chains: deubiquitylating enzyme specificity begets function. *Nat Rev Mol Cell Biol*. 2019;20:338-352.

20. Harrigan JA, Jacq X, Martin NM and Jackson SP. Deubiquitylating enzymes and drug discovery: emerging opportunities. *Nat Rev Drug Discov*. 2018;17:57-78.

21. Zhou ZX, Ren Z, Yan BJ, Qu SL, Tang ZH, Wei DH, Liu LS, Fu MG and Jiang ZS. The Role of Ubiquitin E3 Ligase in Atherosclerosis. *Curr Med Chem*. 2021;28:152-168.

22. Cheng X, Wang K, Zhao Y and Wang K. Research progress on post-translational modification of proteins and cardiovascular diseases. *Cell Death Discov*. 2023;9:275.

23. Cao L, Zhang J, Yu L, Yang W, Qi W, Ren R, Liu Y, Hou Y, Cao Y, Li Q, Wang X, Zhang Z, Li B, Sui W, Zhang Y, Gao C, Zhang C and Zhang M. E3 ubiquitin ligase Listerin regulates macrophage cholesterol efflux and atherosclerosis by targeting ABCA1. *J Clin Invest*. 2025;135.

24. Liu Y, Zhang X, Yu L, Cao L, Zhang J, Li Q, Wang X, Qi W, Cai L, Ren R, Wang W, Guo X, Su G, Xi B, Zhang Y, Gao C, Zhang M and Zhang C. E3 ubiquitin ligase RNF128 promotes Lys63-linked polyubiquitination on SRB1 in macrophages and aggravates atherosclerosis. *Nat Commun*. 2025;16:2185.

25. Zhang J, Yu L, Yang W, Cao L, Wang X, Kao C, Li Z, Ren R, Qi W, Lyu L, Xiong W, Sui W, Wu X, Li N, Liu B, Wang S, Bu P, Zhang Y, Gao C, Zhang C and Zhang M. Macrophage-Specific E3 Ubiquitin Ligase TRIM31 Reduces Atherosclerotic Plaque Formation by Targeting LOX-1. *Circulation*. 2025.

26. Li Q, Ye C, Tian T, Jiang Q, Zhao P, Wang X, Liu F, Shan J and Ruan J. The emerging role of ubiquitin-specific protease 20 in tumorigenesis and cancer therapeutics. *Cell Death Dis*. 2022;13:434.

27. Qin B, Zhou L, Wang F and Wang Y. Ubiquitin-specific protease 20 in human disease: Emerging role and therapeutic implications. *Biochem Pharmacol*. 2022;206:115352.

28. Lu XY, Shi XJ, Hu A, Wang JQ, Ding Y, Jiang W, Sun M, Zhao X, Luo J, Qi W and Song BL. Feeding induces cholesterol biosynthesis via the mTORC1-USP20-HMGCR axis. *Nature*. 2020;588:479-484.

29. Zhang M, Wang Z, Zhao Q, Yang Q, Bai J, Yang C, Zhang ZR and Liu Y. USP20 deubiquitinates and stabilizes the reticulophagy receptor RETREG1/FAM134B to drive reticulophagy. *Autophagy*. 2024;20:1780-1797.

30. Ma C, Li Y, Tian M, Deng Q, Qin X, Lu H, Gao J, Chen M, Weinstein LS, Zhang M, Bu P, Yang J, Zhang Y, Zhang C and Zhang W. Gsalpha Regulates Macrophage Foam Cell Formation During Atherosclerosis. *Circ Res*. 2024;134:e34-e51.

31. Lv F, Fang H, Huang L, Wang Q, Cao S, Zhao W, Zhou Z, Zhou W and Wang X. Curcumin Equipped Nanozyme-Like Metal-Organic Framework Platform for the Targeted Atherosclerosis Treatment with Lipid Regulation and Enhanced Magnetic Resonance Imaging Capability. *Adv Sci (Weinh)*. 2024;11:e2309062.

32. Jean-Charles PY, Wu JH, Zhang L, Kaur S, Nepliouev I, Stiber JA, Brian L, Qi R, Wertman V, Shenoy SK and Freedman NJ. USP20 (Ubiquitin-Specific Protease 20) Inhibits TNF (Tumor Necrosis Factor)-Triggered Smooth Muscle Cell Inflammation and Attenuates Atherosclerosis. *Arterioscler Thromb Vasc Biol*. 2018;38:2295-2305.

33. Zhang L, Wu JH, Jean-Charles PY, Murali P, Zhang W, Jazic A, Kaur S, Nepliouev I, Stiber JA, Snow K, Freedman NJ and Shenoy SK. Phosphorylation of USP20 on Ser334 by IRAK1 promotes IL-1beta-evoked signaling in vascular smooth muscle cells and vascular inflammation. *J Biol Chem*. 2023;299:104911.

34. Chen Y, Yang M, Huang W, Chen W, Zhao Y, Schulte ML, Volberding P, Gerbec Z, Zimmermann MT,

Zeighami A, Demos W, Zhang J, Knaack DA, Smith BC, Cui W, Malarkannan S, Sodhi K, Shapiro JI, Xie Z, Sahoo D and Silverstein RL. Mitochondrial Metabolic Reprogramming by CD36 Signaling Drives Macrophage Inflammatory Responses. *Circ Res*. 2019;125:1087-1102.

35. Kumar A, Gupta P, Rana M, Chandra T, Dikshit M and Barthwal MK. Role of pyruvate kinase M2 in oxidized LDL-induced macrophage foam cell formation and inflammation. *J Lipid Res*. 2020;61:351-364.

36. Babaev VR, Runner RP, Fan D, Ding L, Zhang Y, Tao H, Erbay E, Gorgun CZ, Fazio S, Hotamisligil GS and Linton MF. Macrophage Mal1 deficiency suppresses atherosclerosis in low-density lipoprotein receptor-null mice by activating peroxisome proliferator-activated receptor-gamma-regulated genes. *Arterioscler Thromb Vasc Biol*. 2011;31:1283-90.

37. Kou F, Li XY, Feng Z, Hua J, Wu X, Gao H, Lin J, Kang D, Li A, Li J, Ding Y, Ban T, Zhang Q and Liu Z. GPR171 restrains intestinal inflammation by suppressing FABP5-mediated Th17 cell differentiation and lipid metabolism. *Gut*. 2025;74:1279-1292.

38. Cochain C, Vafadarnejad E, Arampatzi P, Pelisek J, Winkels H, Ley K, Wolf D, Saliba AE and Zernecke A. Single-Cell RNA-Seq Reveals the Transcriptional Landscape and Heterogeneity of Aortic Macrophages in Murine Atherosclerosis. *Circ Res*. 2018;122:1661-1674.

39. Wirka RC, Wagh D, Paik DT, Pjanic M, Nguyen T, Miller CL, Kundu R, Nagao M, Coller J, Koyano TK, Fong R, Woo YJ, Liu B, Montgomery SB, Wu JC, Zhu K, Chang R, Alamprese M, Tallquist MD, Kim JB and Quertermous T. Atheroprotective roles of smooth muscle cell phenotypic modulation and the TCF21 disease gene as revealed by single-cell analysis. *Nat Med*. 2019;25:1280-1289.

40. Hotamisligil GS and Bernlohr DA. Metabolic functions of FABPs--mechanisms and therapeutic implications. *Nat Rev Endocrinol*. 2015;11:592-605.

41. Tontonoz P, Nagy L, Alvarez JG, Thomazy VA and Evans RM. PPARgamma promotes monocyte/macrophage differentiation and uptake of oxidized LDL. *Cell*. 1998;93:241-52.

42. Desvergne B. PPARdelta/beta: the lobbyist switching macrophage allegiance in favor of metabolism. *Cell Metab*. 2008;7:467-9.

43. Zhong L, Dai S, Yu F, Shi GP, Gong Q, Zhang Y, Duan J, Lou Z, Tang Z, Gong F, Chen D, Hou L, Hu X, Chen J, Wang J and Yin D. Cardiomyocyte-Enriched USP20 Ameliorates Pathological Cardiac Hypertrophy by Targeting STAT3 Deubiquitination. *Adv Sci (Weinh)*. 2025;12:e2416478.

44. Yeung DC, Wang Y, Xu A, Cheung SC, Wat NM, Fong DY, Fong CH, Chau MT, Sham PC and Lam KS. Epidermal fatty-acid-binding protein: a new circulating biomarker associated with cardio-metabolic risk factors and

carotid atherosclerosis. *Eur Heart J*. 2008;29:2156-63.

45. Furuhashi M, Ogura M, Matsumoto M, Yuda S, Muranaka A, Kawamukai M, Omori A, Tanaka M, Moniwa N, Ohnishi H, Saitoh S, Harada-Shiba M, Shimamoto K and Miura T. Serum FABP5 concentration is a potential biomarker for residual risk of atherosclerosis in relation to cholesterol efflux from macrophages. *Sci Rep*. 2017;7:217.

46. Bagheri R, Qasim AN, Mehta NN, Terembula K, Kapoor S, Braunstein S, Schutta M, Iqbal N, Lehrke M and Reilly MP. Relation of plasma fatty acid binding proteins 4 and 5 with the metabolic syndrome, inflammation and coronary calcium in patients with type-2 diabetes mellitus. *Am J Cardiol*. 2010;106:1118-23.

47. Hou Y, Wei D, Zhang Z, Guo H, Li S, Zhang J, Zhang P, Zhang L and Zhao Y. FABP5 controls macrophage alternative activation and allergic asthma by selectively programming long-chain unsaturated fatty acid metabolism. *Cell Rep*. 2022;41:111668.

48. Yang X, Deng B, Zhao W, Guo Y, Wan Y, Wu Z, Su S, Gu J, Hu X, Feng W, Hu C, Li J, Xu Y, Huang X and Lin Y. FABP5(+) lipid-loaded macrophages process tumour-derived unsaturated fatty acid signal to suppress T-cell antitumour immunity. *J Hepatol*. 2025;82:676-689.

49. Guo Y, Liu Y, Zhao S, Xu W, Li Y, Zhao P, Wang D, Cheng H, Ke Y and Zhang X. Oxidative stress-induced FABP5 S-glutathionylation protects against acute lung injury by suppressing inflammation in macrophages. *Nat Commun*. 2021;12:7094.

50. Li X, He W, Chen X, Zhang Y, Zhang J, Liu F, Li J, Zhao D, Xia P, Ma W, Wu T, Wang H and Yuan Y. TRIM45 facilitates NASH-progressed HCC by promoting fatty acid synthesis via catalyzing FABP5 ubiquitylation. *Oncogene*. 2024;43:2063-2077.

51. Qian J, Zhao Z, Ma L, Liu W and Song Y. USP14 targets FABP5-mediated ferroptosis to promote proliferation and cisplatin resistance of HNSCC. *Clin Transl Oncol*. 2025;27:3485-3500.

52. Costet P, Luo Y, Wang N and Tall AR. Sterol-dependent transactivation of the ABC1 promoter by the liver X receptor/retinoid X receptor. *J Biol Chem*. 2000;275:28240-5.

53. Zelcer N and Tontonoz P. Liver X receptors as integrators of metabolic and inflammatory signaling. *J Clin Invest*. 2006;116:607-14.

54. Pirillo A, Norata GD and Catapano AL. LOX-1, OxLDL, and atherosclerosis. *Mediators Inflamm*. 2013;2013:152786.

55. Sarraju A and Nissen SE. Atherosclerotic plaque stabilization and regression: a review of clinical evidence. *Nat Rev Cardiol*. 2024;21:487-497.

56. Vrints C, Andreotti F, Koskinas KC, Rossello X, Adamo M, Ainslie J, Banning AP, Budaj A, Buechel RR,

Chiariello GA, Chieffo A, Christodorescu RM, Deaton C, Doenst T, Jones HW, Kunadian V, Mehilli J, Milojevic M, Piek JJ, Pugliese F, Rubboli A, Semb AG, Senior R, Ten Berg JM, Van Belle E, Van Craenenbroeck EM, Vidal-Perez R, Winther S and Group ESCSD. 2024 ESC Guidelines for the management of chronic coronary syndromes. *Eur Heart J*. 2024;45:3415-3537.

57. Chen W, Schilperoort M, Cao Y, Shi J, Tabas I and Tao W. Macrophage-targeted nanomedicine for the diagnosis and treatment of atherosclerosis. *Nat Rev Cardiol*. 2022;19:228-249.

58. Galindo CL, Khan S, Zhang X, Yeh YS, Liu Z and Razani B. Lipid-laden foam cells in the pathology of atherosclerosis: shedding light on new therapeutic targets. *Expert Opin Ther Targets*. 2023;27:1231-1245.

## Figures with Figure Legends

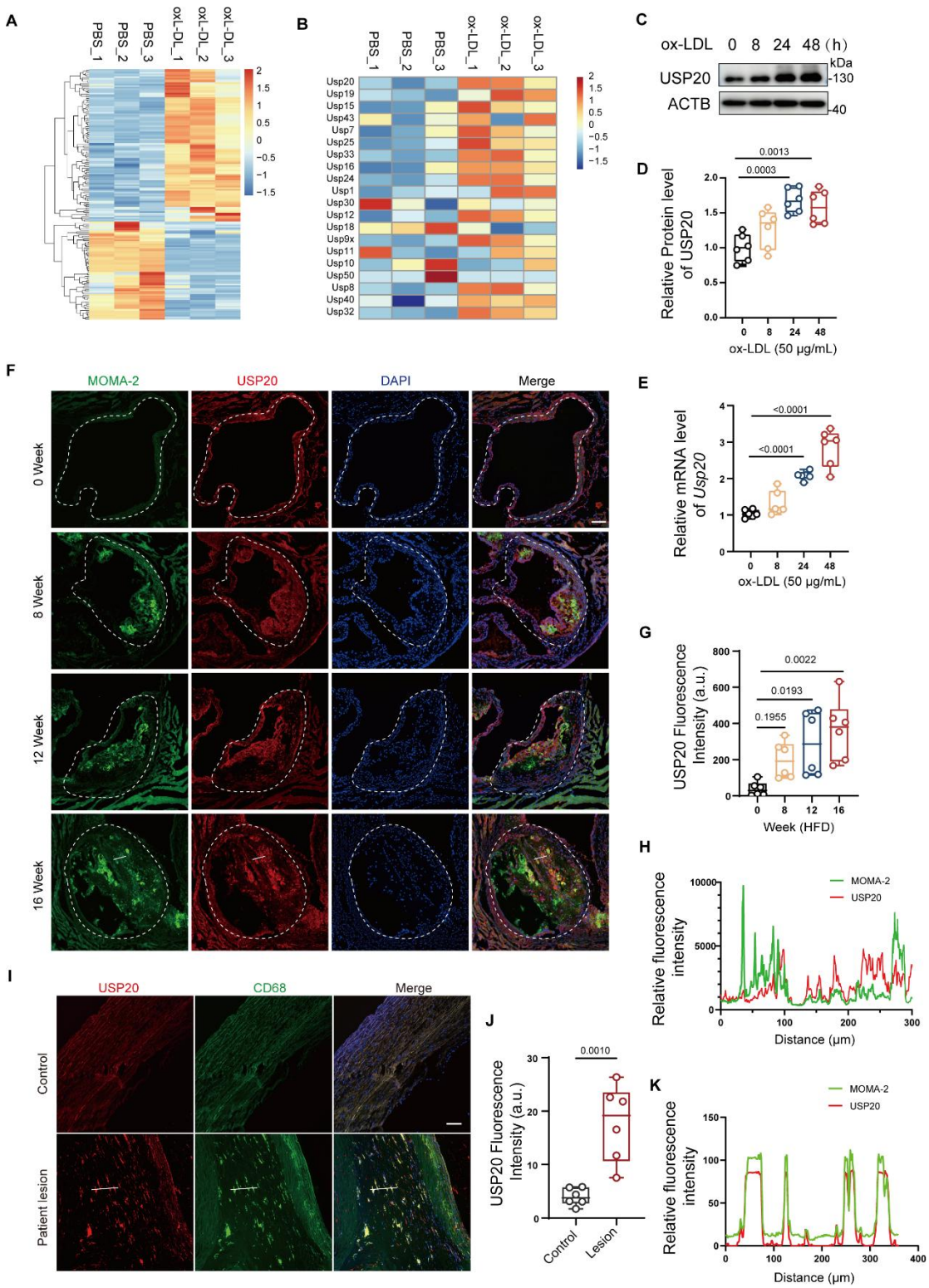


**Figure 1. USP20 is upregulated in macrophages and atherosclerotic lesions during atherosclerosis progression.**

**(A)** Heatmap showing differentially expressed genes in bone marrow-derived macrophages (BMDMs) treated with PBS or ox-LDL, as determined by RNA sequencing. **(B)** Heatmap showing

762 the expression profiles of selected DUBs altered in response to ox-LDL stimulation. **(C–E)** BMDMs
763 were stimulated with ox-LDL (50 μg/mL) for the indicated time periods. Representative
764 immunoblot (C) and quantitative analysis (D) showing USP20 protein expression. Quantitative RT-
765 PCR analysis showing relative *Usp20* mRNA expression (E), n = 6. **(F–H)** Immunofluorescence
766 staining of USP20 (red), the macrophage marker MOMA-2 (green), and nuclei (DAPI, blue) in
767 aortic root sections collected from mice fed a Paigen diet for 0, 8, 12, or 16 weeks following AAV-
768 PCSK9 injection (F). Representative images are shown. Quantification of USP20 fluorescence
769 intensity during lesion progression (G). Representative fluorescence intensity profile demonstrating
770 the spatial colocalization of USP20 and MOMA-2 signals (H). **(I–K)** Immunofluorescence staining
771 of USP20 (red) and CD68 (green) in paired human carotid endarterectomy specimens, including
772 adjacent non-plaque arterial regions (Control) and atherosclerotic plaque regions (Patient lesion) (I).
773 Quantification of USP20 fluorescence intensity (J). Representative fluorescence intensity profile
774 showing the spatial colocalization of USP20 and CD68 signals (K). Data are presented as mean ±
775 SEM. Statistical significance was determined using paired two-tailed Student's t test (J) and one-
776 way ANOVA followed by Tukey's multiple-comparison test (D, E, and G). Scale bars, 100 μm (F
777 and I).

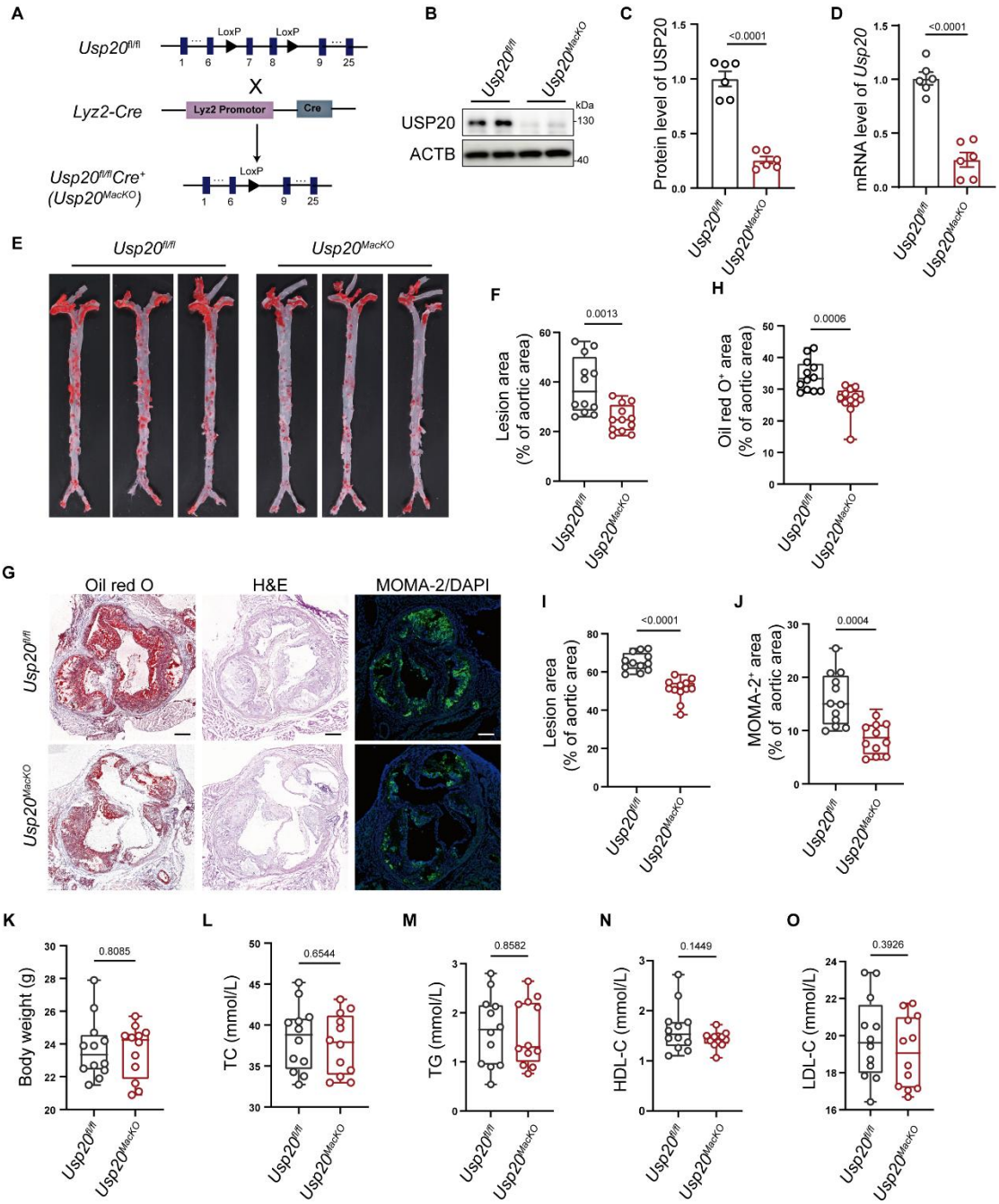


**Figure 2. Macrophage *Usp20* deficiency protects against atherosclerotic plaque formation *in vivo*.**

**(A)** Schematic illustration of the generation of macrophage-specific *USP20* knockout mice (*Usp20*$^{\text{MacKO}}$) by crossing *Usp20*$^{\text{fl/fl}}$ mice with *Lyz2*-Cre mice. **(B–D)** Validation of USP20 deletion in bone marrow-derived macrophages (BMDMs). Representative immunoblot (B) and quantitative analysis (C) showing USP20 protein expression. Quantitative RT-PCR analysis of *Usp20* mRNA levels (D), n = 6. **(E–F)** Representative en face Oil Red O staining of the entire aorta from *Usp20*$^{\text{fl/fl}}$

786 and *Usp20*$^{MacKO}$ mice following AAV-PCSK9 injection and 12 weeks of Paigen diet feeding (E).
787 Quantification of aortic lesion area is shown (F), n = 12. **(G–J)** Representative Oil Red O,
788 hematoxylin and eosin (H&E), and immunofluorescence staining for MOMA-2 (green) with DAPI
789 (blue) in aortic root sections (G). Quantification of Oil Red O-positive lesion area (H), total lesion
790 area determined from H&E staining (I), and MOMA-2-positive macrophage area (J), n = 12. **(K–**
791 **O)** Body weight (K) and plasma lipid profiles, including total cholesterol (TC, L), triglycerides (TG,
792 M), high-density lipoprotein cholesterol (HDL-C, N), and low-density lipoprotein cholesterol
793 (LDL-C, O), measured at the experimental endpoint, n = 12. Data are presented as mean ± SEM.
794 Statistical significance was determined using unpaired two-tailed Student's t test. Scale bars, 200
795 μm (G).

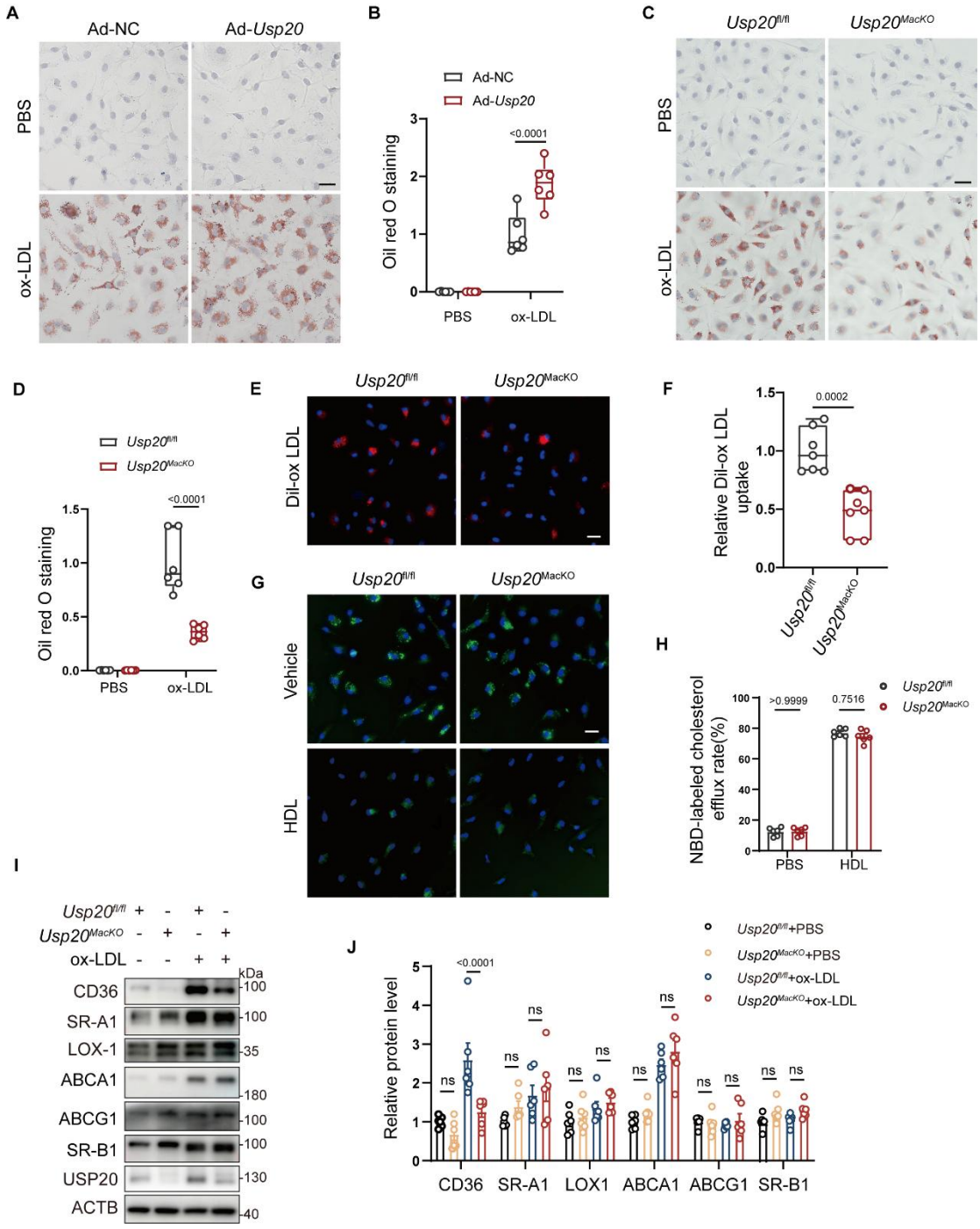


**Figure 3. USP20 drives macrophage foam cell formation by promoting CD36-dependent lipid uptake.**

**(A–B)** Representative Oil Red O staining (A) and quantification (B) of lipid accumulation in BMDMs transduced with adenovirus expressing USP20 (Ad-*Usp20*) or control adenovirus (Ad-NC) following ox-LDL stimulation, n = 6. **(C–D)** Representative Oil Red O staining (C) and quantitative analysis (D) of lipid accumulation in *Usp20*$^{fl/fl}$ and *Usp20*$^{MacKO}$ BMDMs treated with ox-LDL, n = 6. **(E–F)** Representative fluorescence images (E) and quantification (F) of DiI-labeled ox-LDL

uptake in *Usp20*$^{fl/fl}$ and *Usp20*$^{MacKO}$ BMDMs, n = 6. **(G–H)** Representative fluorescence images (G) and quantitative analysis (H) of NBD-cholesterol efflux to HDL in *Usp20*$^{fl/fl}$ and *Usp20*$^{MacKO}$ BMDMs, n = 6. **(I–J)** Representative immunoblot (I) and densitometric quantification (J) of proteins involved in lipid uptake and cholesterol efflux, including CD36, SR-A1, LOX-1, ABCA1, ABCG1, and SR-B1, in *Usp20*$^{fl/fl}$ and *Usp20*$^{MacKO}$ BMDMs following ox-LDL stimulation, n = 6. Data are presented as mean ± SEM. Statistical significance was determined using unpaired two-tailed Student's *t* test (B, D, F, and H) or two-way ANOVA followed by Tukey's multiple-comparison test (J). Scale bars, 20 μm (A, C, E, and G).

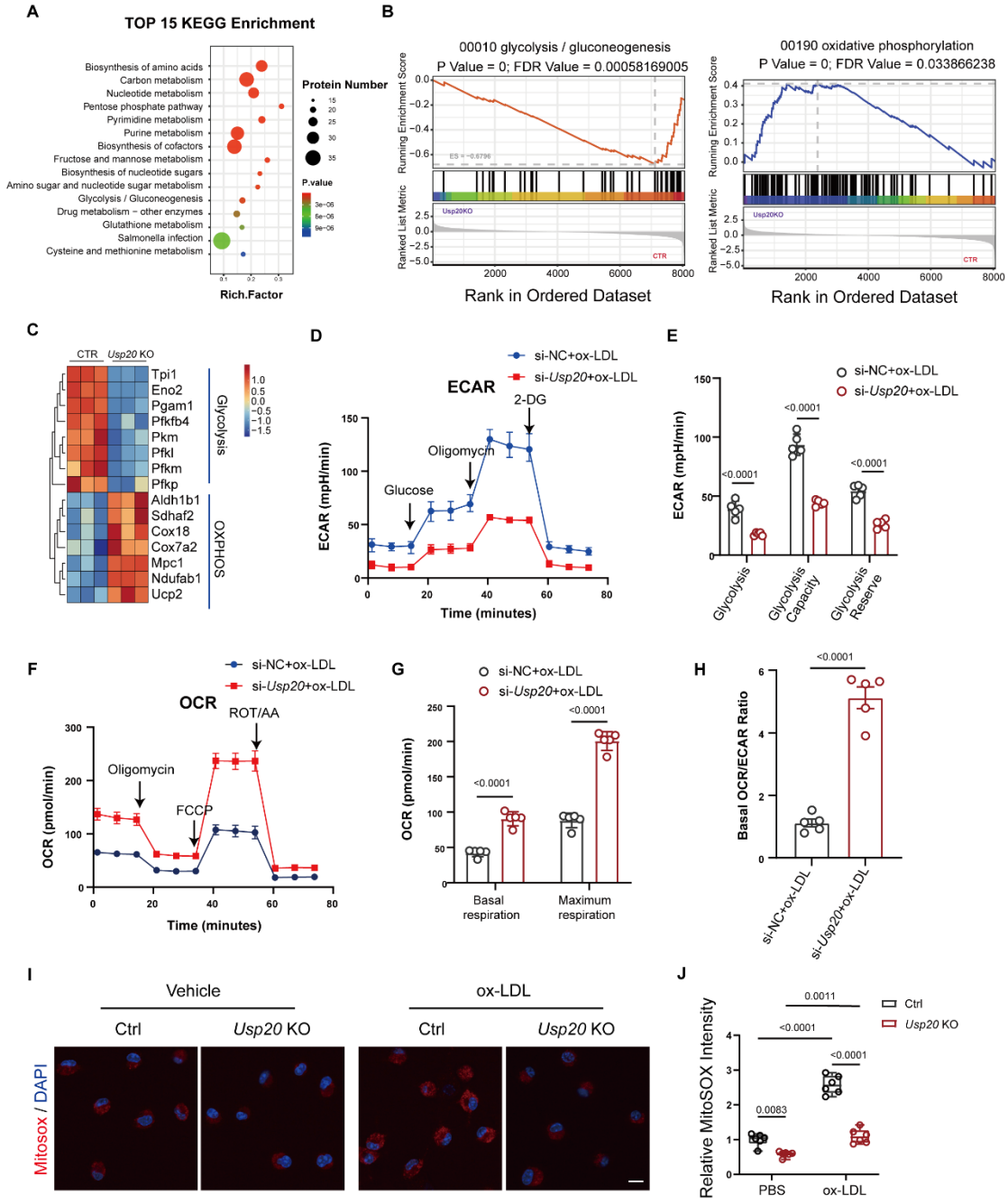

**Figure 4. *Usp20* deficiency is associated with improved mitochondrial metabolic homeostasis during foam cell formation.**

**(A)** KEGG pathway enrichment analysis of differentially expressed proteins identified by quantitative proteomic analysis of *Usp20*-deficient macrophages. **(B)** Gene set enrichment analysis (GSEA) showing significant enrichment of glycolysis/gluconeogenesis and oxidative phosphorylation pathways in *Usp20*-deficient macrophages. **(C)** Heatmap showing the expression of representative proteins involved in glycolysis and oxidative phosphorylation identified by proteomic analysis. **(D–E)** Extracellular acidification rate (ECAR) analysis of BMDMs transfected with control siRNA (si-NC) or si-*Usp20*. Representative glycolytic stress test profiles (D) and quantification of glycolysis, glycolytic capacity, and glycolytic reserve (E). **(F–H)** Oxygen consumption rate (OCR) analysis of BMDMs transfected with si-NC or si-*Usp20*. Representative mitochondrial stress test profiles (F) and quantification of basal and maximal respiration (G) and the basal OCR/ECAR ratio (H). **(I–J)** Representative MitoSOX fluorescence images (I) and quantitative analysis (J) of mitochondrial reactive oxygen species (mtROS) levels in control and *Usp20*-deficient BMDMs under basal conditions or following ox-LDL stimulation. Data are presented as mean ± SEM. Statistical significance was determined using unpaired two-tailed Student's *t* test (E, G, and H) or two-way ANOVA followed by Tukey's multiple-comparison test (J). Scale bars, 20 μm (I).

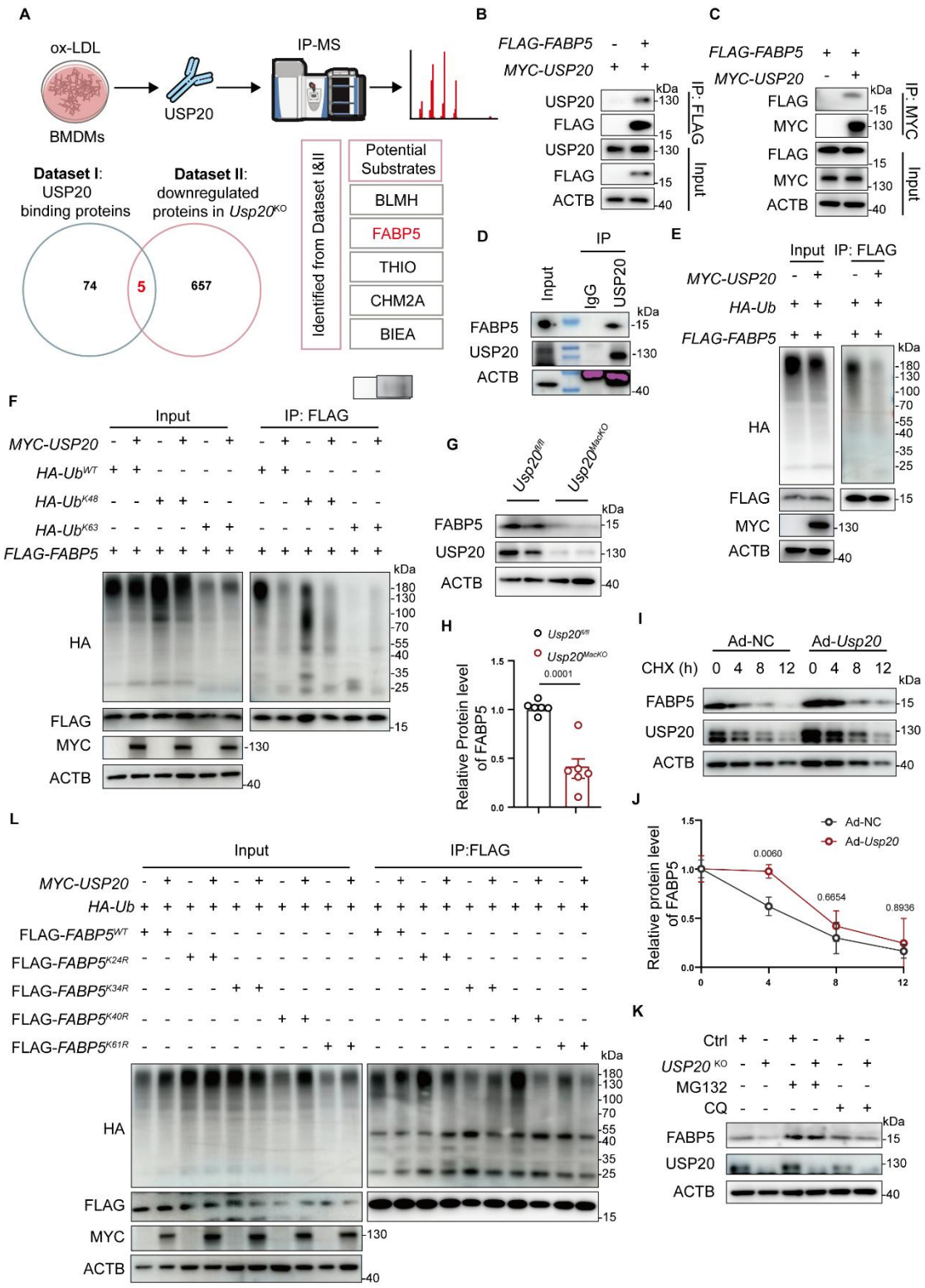


**Figure 5. USP20 stabilizes FABP5 through K48-linked deubiquitination.**

**(A)** Schematic illustration of the substrate screening strategy. USP20-interacting proteins identified by immunoprecipitation coupled with mass spectrometry (IP-MS) were intersected with proteins downregulated in *Usp20*-deficient macrophages identified by quantitative proteomics, yielding five

candidate USP20 substrates, including FABP5. **(B–D)** Interaction between USP20 and FABP5. Co-immunoprecipitation (Co-IP) of ectopically expressed MYC-USP20 and FLAG-FABP5 in HEK293T cells (B, C) and endogenous Co-IP of USP20 and FABP5 in BMDMs (D). **(E)** In vivo ubiquitination assay showing that USP20 overexpression decreases the ubiquitination of FABP5. **(F)** Ubiquitination assays using wild-type, K48-linked, or K63-linked ubiquitin constructs demonstrating that USP20 specifically removes K48-linked polyubiquitin chains from FABP5. **(G–H)** Representative immunoblot (G) and quantitative analysis (H) showing reduced FABP5 protein expression in *Usp20*$^{\mathrm{MacKO}}$ BMDMs, n = 6. **(I–J)** Cycloheximide (CHX) chase assay showing that USP20 overexpression prolongs the half-life of FABP5 protein. Representative immunoblot (I) and quantitative analysis (J), n = 4. **(K)** Immunoblot analysis showing that MG132, but not chloroquine (CQ), restores FABP5 protein abundance in *Usp20*-deficient macrophages, indicating proteasome-dependent degradation of FABP5. **(L)** Ubiquitination assays using FLAG-FABP5 lysine mutants (K24R, K34R, K40R, and K61R) identifying Lys34 as the major ubiquitination site regulated by USP20. Data are presented as mean ± SEM. Statistical significance was determined using unpaired two-tailed Student's *t* test (H) or two-way ANOVA followed by Tukey's multiple-comparison test (J).

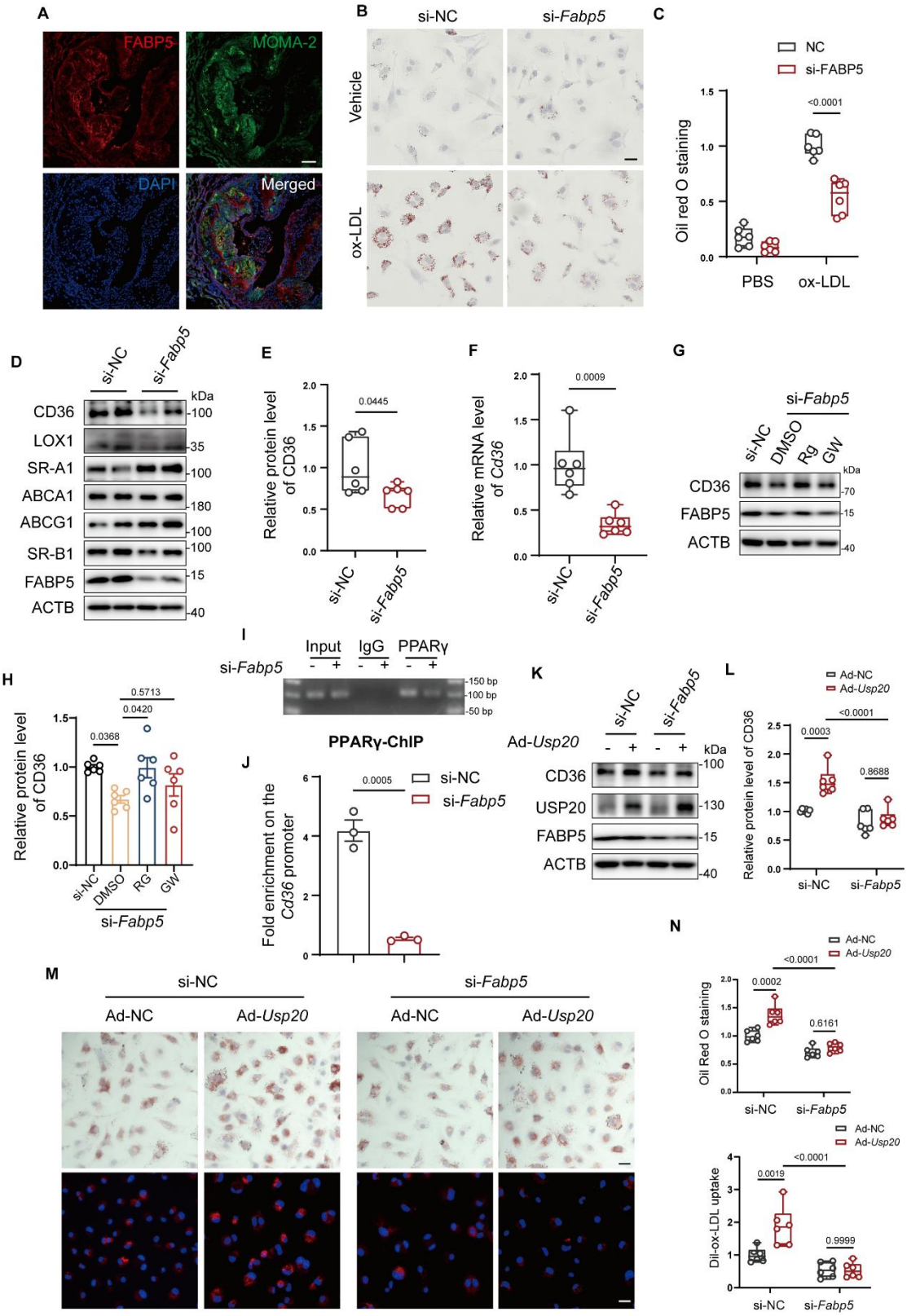


**Figure 6. FABP5 mediates USP20-dependent activation of the PPARγ–CD36 axis and macrophage foam cell formation.**

**(A)** Representative immunofluorescence staining of FABP5 (red), MOMA-2 (green), and nuclei

856 (DAPI, blue) in aortic root sections from atherosclerotic mice. **(B–C)** Representative Oil Red O
857 staining (B) and quantitative analysis (C) of lipid accumulation in BMDMs transfected with si-NC
858 or si-*Fabp5* following ox-LDL stimulation, n = 6. **(D–F)** Representative immunoblot (D) and
859 quantitative analysis of CD36 protein (E) and *Cd36* mRNA (F) expression in BMDMs transfected
860 with si-NC or si-*Fabp5* after ox-LDL treatment, n = 6. **(G–H)** Immunoblot analysis (G) and
861 quantitative densitometric analysis (H) of CD36 protein expression in si-*Fabp5* BMDMs treated
862 with the PPARγ agonist rosiglitazone (RG) or the PPARβ/δ agonist GW501516 (GW), n = 6. **(I–J)**
863 Representative agarose gel image (I) and quantitative ChIP-qPCR analysis (J) showing PPARγ
864 binding to the *Cd36* promoter in BMDMs transfected with si-NC or si-*Fabp5*, n = 3. **(K–L)**
865 Representative immunoblot (K) and quantitative analysis (L) of CD36 protein expression in
866 BMDMs following *Usp20* overexpression with or without *Fabp5* knockdown, n = 6. **(M–N)**
867 Representative Oil Red O staining and DiI-labeled ox-LDL uptake images (M) and quantitative
868 analysis (N) in BMDMs following *Usp20* overexpression in the presence or absence of *Fabp5*
869 knockdown, n = 6. Data are presented as mean ± SEM. Statistical significance was determined using
870 unpaired two-tailed Student's *t* test (E, F, and J), one-way ANOVA followed by Tukey's multiple-
871 comparison test (H) or two-way ANOVA followed by Tukey's multiple-comparison test (C, L and
872 N). Scale bars, 100 μm (A) and 20 μm (B and M).

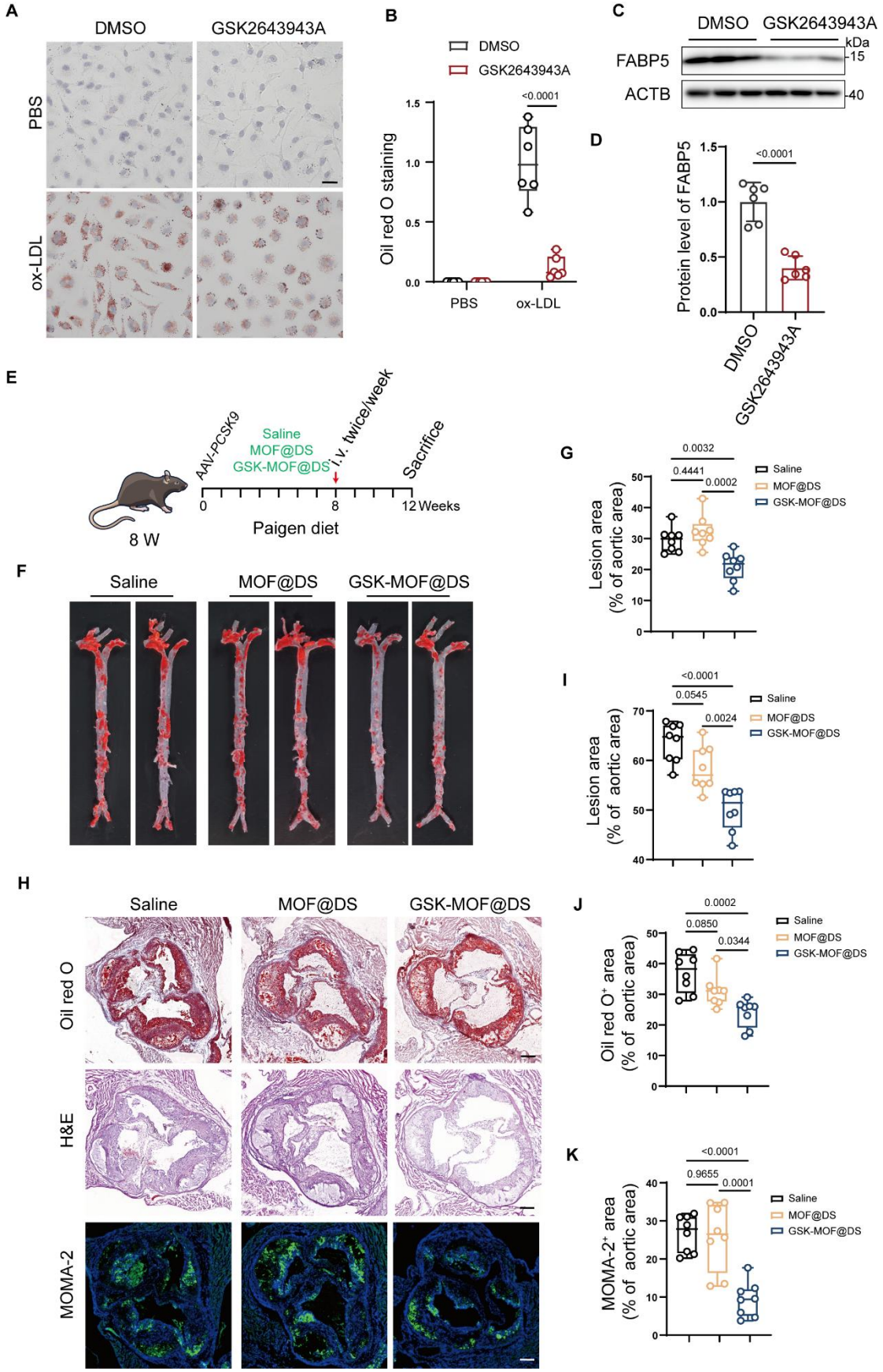


873

874 **Figure 7. Pharmacological inhibition of USP20 suppresses macrophage foam cell**

**formation and attenuates atherosclerosis.**

**(A–D)** Effects of the USP20 inhibitor GSK2643943A on macrophage foam cell formation in vitro. Representative Oil Red O staining (A) and quantitative analysis (B) of lipid accumulation in ox-LDL-treated BMDMs following treatment with GSK2643943A. Representative immunoblot (C) and quantitative analysis (D) showing reduced FABP5 protein expression after USP20 inhibition, n = 6. **(E)** Schematic illustration of the experimental protocol. Eight-week-old mice were injected with AAV-PCSK9 and fed a Paigen diet for 12 weeks. Saline, empty MOF nanoparticles (MOF@DS), or GSK2643943A-loaded MOF nanoparticles (GSK-MOF@DS) were administered intravenously twice weekly beginning at week 8. **(F–G)** Representative en face Oil Red O staining of the entire aorta (F) and quantification of aortic lesion area (G) in mice treated with saline, MOF@DS, or GSK-MOF@DS, n = 8. **(H–K)** Representative Oil Red O staining, hematoxylin and eosin (H&E) staining, and immunofluorescence staining for MOMA-2 (green) with DAPI (blue) in aortic root sections (H). Quantification of total lesion area (I), Oil Red O-positive lesion area (**J**), and MOMA-2-positive macrophage area (K), n = 8. Data are presented as mean ± SEM. Statistical significance was determined using unpaired two-tailed Student's *t* test (D), one-way ANOVA followed by Tukey's multiple-comparison test (G, I, J, and K) or two-way ANOVA followed by Tukey's multiple-comparison test (B). Scale bars, 100 μm (H) and 20 μm (A).

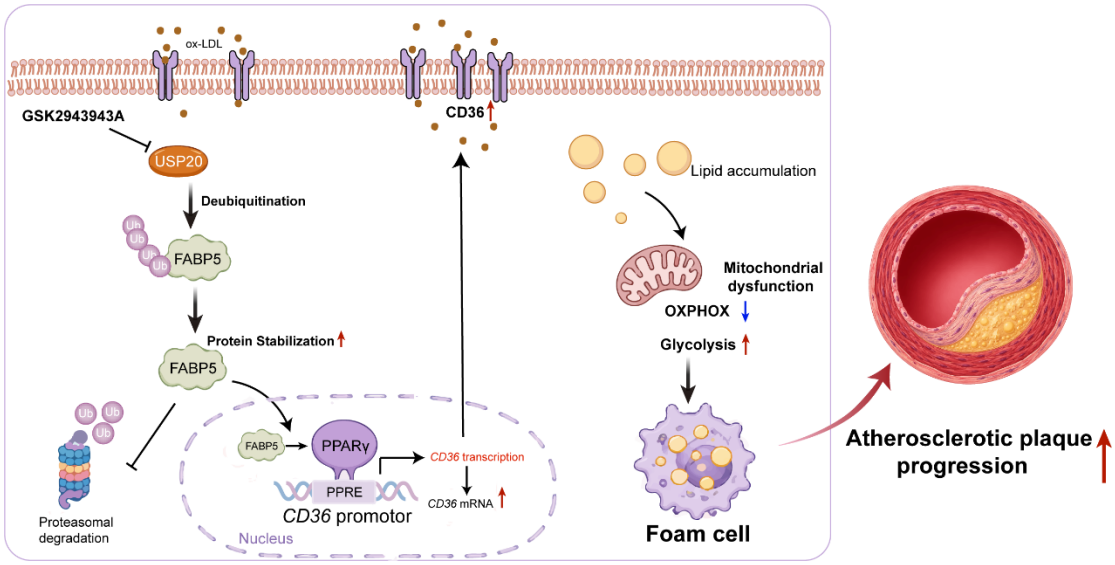


**Figure 8. USP20 promotes macrophage foam cell formation and atherosclerosis through the FABP5–PPARγ–CD36 axis axis.**

Oxidized low-density lipoprotein (ox-LDL) induces USP20 expression in macrophages. USP20

directly deubiquitinates FABP5, thereby preventing its proteasomal degradation and increasing FABP5 protein stability. Stabilized FABP5 enhances PPARγ-dependent transcription of *CD36*, leading to elevated CD36 expression and increased ox-LDL uptake. Excessive lipid accumulation is associated with mitochondrial dysfunction and metabolic reprogramming, characterized by impaired oxidative phosphorylation and enhanced glycolysis, which may further promote macrophage foam cell formation. Therapeutically, macrophage-targeted delivery of the USP20 inhibitor GSK2643943A using a metal-organic framework nanoplatform (GSK-MOF@DS) suppresses USP20 activity, reduces FABP5 protein abundance, inhibits foam cell formation, and attenuates atherosclerotic lesion development.